Applied Physics Letters ARTICLE scitation.org/journal/apl

Electronic transport in copper–graphene composites

Cite as: Appl. Phys. Lett. **122**, 031903 (2023); doi: 10.1063/5.0137086
Submitted: 30 November 2022 · Accepted: 7 January 2023 ·
Published Online: 19 January 2023

Kashi N. Subedi,[1] Kishor Nepal,[1] Chinonso Ugwumadu,[1] Keerti Kappagantula,[2] and D. A. Drabold[1,a)]

AFFILIATIONS

[1]Department of Physics and Astronomy, Ohio University, Athens, Ohio 45701, USA
[2]Pacific Northwest National Laboratory, Richland, Washington 99352, USA

[a)]Author to whom correspondence should be addressed: drabold@ohio.edu

ABSTRACT

We investigate electronic transport properties of copper–graphene (Cu–G) composites using a density-functional theory (DFT) framework. Conduction in composites is studied by varying the interfacial distance of copper/graphene/copper (Cu/G/Cu) interface models. Electronic conductivity of the models computed using the Kubo–Greenwood formula shows that the conductivity increases with decreasing Cu–G distance and saturates below a threshold Cu–G distance. The DFT-based Bader charge analysis indicates increasing charge transfer between Cu atoms at the interfacial layers and the graphene with decreasing Cu–G distance. The electronic density of states reveals increasing contributions from both copper and carbon atoms near the Fermi level with decreasing Cu–G interfacial distance. By computing the space-projected conductivity of the Cu/G/Cu models, we show that the graphene forms a bridge to the electronic conduction at small Cu–G distances, thereby enhancing the conductivity.

Metal composites are key industrial materials that may be manufactured using various novel techniques,[1–3] leading to metastable materials exhibiting desirable mechanical, thermal, electronic, and transport properties without the constraints typically seen in alloys. Copper is used extensively for energy transport and electromagnetic applications such as motors, generators, cables, busbars, and transformers. In the last two decades, we have witnessed copper composites with improved transport properties,[4] devised as a means to reduce energy loss in applications.

One material that has demonstrated improved electrical conductivity and current density is a copper–graphene (Cu–G) composite. Various Cu–G composites ranging from a simple interface laminated to bulk Cu with interconnected graphene flakes have been reported in the literature with some showing enhanced conductivity[5–8] and more commonly showing enhancement in mechanical performance.[7,9] Conventional wisdom suggests that the introduction of additives to metal would increase scattering that would lead to increased electrical resistivity.[10] This is the reason why addition of silver to copper leads to reduced electrical conductivity of Cu, even though Ag is 8% higher in conductivity than Cu.[11] The additives, on the other hand, also arrest dislocation movement in the metals due to several mechanisms such as precipitate hardening, solid solution strengthening, and dispersion strengthening, resulting in enhanced mechanical performance.[12]

At this juncture, it is known that the electrical conductivity of the Cu–G composites is dependent on the quantity of graphene used in the composites, the type of graphene and their defect density, and the arrangement of the Cu matrix and graphene in the composite microstructure, which eventually dictates the carrier transport in the material during conduction.[13,14] Processing routes adopted to manufacture the composites are also known to influence electrical performance. Processes that can control atomic scale deposition of Cu and graphene, such as vapor deposition and molecular beam epitaxy, have shown promise in manufacturing nano-to-micron scale samples demonstrating enhanced electrical performance.[15] At the bulk scale, solid phase processing techniques have shown promise in enhancing electrical conductivity.[13]

In all this, however, while there is an evolving understanding of processing approaches and material chemistries that result in Cu–G composites with improved electrical performance, little is known about the nature of charge-carrier transfer between Cu and graphene. Several papers discussed carrier mobility in graphene that is deposited on Cu foils.[16,17] However, limited experimental and computational research is published on transport phenomena across metal/graphene interfaces. There is minimal understanding of how the nature of the interface (such as atom arrangement and interfacial distance) affects the electron density at the interface. In Cu–G composites

demonstrating enhanced conductivity compared to the corresponding Cu substrates, two causes were hypothesized for the enhancement in conductivity. In one case, where the manufacturing conditions allow for it, the Cu grains are surmised to be templated on the adjacent graphene flakes leading to the formation of predominantly 111 textures in the composite during the manufacturing process. Such crystallographic orientations in Cu show higher conductivity compared to other textures such as 200 or 110. If there is a large concentration of 111 grains in the Cu microstructure, it is reasonable to expect an enhanced conductivity overall. In this hypothesis, graphene is thought to only template the grains but not actually participate in the conduction process. In the second case, graphene is assumed to participate during conduction through the exchange of carriers with the surrounding Cu matrix. One key consideration for this hypothesis is the nature of interface between Cu and graphene that may be suitable for carrier transport across the interface. Some papers indicated that the 111 Cu grains offer the least lattice mismatch with graphene, which may also help with carrier transport. However, it is currently not well known how much conductivity the introduction of graphene brings about for Cu per this hypothesis.

In this Letter, we explore the electrical transport properties of the Cu–G composites as a function of the interfacial distance between Cu and graphene, a parameter that can be modulated during Cu–G manufacturing and a simple proxy for a possible strained local configuration. We quantify the electronic transport by computing the electronic conductivity using the Kubo–Greenwood formula (KGF),[18,19] ideally suited for density-functional simulations of materials with its single particle Kohn–Sham orbitals and energies.[20] The KGF method has been utilized in tight-binding and density-functional theory (DFT) computations of the conductivity of liquids and solids.[21,22] We also quantify the charge transport in the composites by computing net charges on interfacial Cu atoms and the graphene using Bader charge analysis.[23,24] In addition to quantifying the conductivity, we determine the conduction-active sites in the Cu–G composites by projecting the KGF conductivity onto real space using the space-projected conductivity (SPC), described elsewhere.[25] The method has been implemented to study conduction processes in crystalline systems with defects, amorphous and semi-conducting systems at the atomistic level.[26–29]

We simulated the Cu–G composite by constructing an interface model with geometry of the form copper/graphene/copper (Cu/G/Cu) as shown in Fig. 1. We adopted one of the low-indexed surfaces, namely, 111, to construct the Cu surface with dimension 10.22×13.28 Å^2. We placed the graphene with one sub-lattice site (A) above the top of the first layer of Cu 111 and the other sub-lattice site (B) placed above the third layer of Cu 111 (refer to Fig. 1). This arrangement is also known as top-fcc and has shown to represent the low-energy structure for Cu–G surface models.[30] The interface model with fcc-top-fcc stacking was then constructed, which has shown to represent the low-energy interface models among six different stackings, namely, fcc–top–fcc, hcp–top–fcc, top–top–fcc, fcc–top–hcp, hcp–top–hcp, and top–top–hcp.[30] We simulated the external pressure on Cu–G composites by varying the Cu–G distance (d_{Cu-G}) of the Cu/G/Cu interface model (refer to Fig. 1). In addition to Cu/G/Cu models, we also constructed an orthorhombic supercell of 216 atoms with the same surface dimension as that of Cu/G/Cu interface models and simulated the external pressure by reducing the vertical dimension

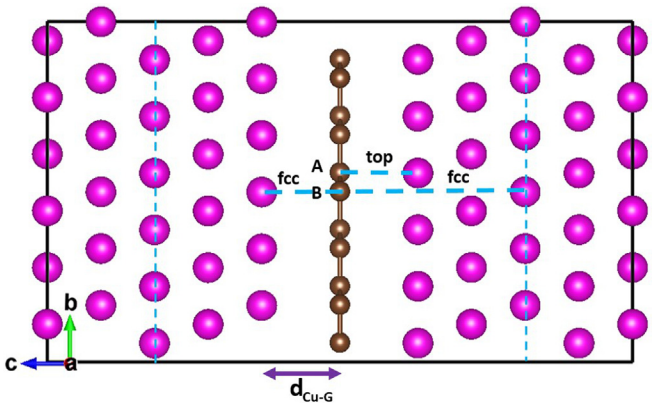

FIG. 1. Geometry of the Cu/G/Cu model with d_{Cu-G} representing the Cu–G distance. Top–fcc configuration of graphene above the Cu 111 surface with A and B representing sub-lattice sites above the Cu atom at first and third layers, respectively. The pink and brown colored spheres represent Cu and C atoms, respectively.

of the supercell. A similar approach has been used to simulate copper and aluminum under external pressure in earlier work.[31]

DFT calculations were carried out using the Vienna *Ab Initio* simulation package[32] (VASP) code. For atomic structure relaxations of Cu/G/Cu models, we used a plane wave basis set with a kinetic energy cutoff of 400 eV. For static calculations, we used a larger cutoff of 520 eV. Projected augmented wave (PAW)[33] potentials were used to account for ion–election interactions, and the generalized gradient approximation of Perdew–Burke–Ernzerhof (PBE)[34] as the exchange-correlation functional. The Brillouin zone sampling was performed using the Monkhorst-Pack scheme with $2 \times 2 \times 1$ **k**-point meshes except for computing electronic density of states (EDOS), where denser **k**-point meshes of $4 \times 4 \times 2$ were used. The periodic boundary conditions were implemented throughout. To determine the partial occupancy of electrons near the Fermi level, the Fermi–Dirac distribution function with a smearing temperature of 1000 K was considered. The δ function in the expression of the KGF was approximated by a Gaussian distribution function of width 0.05 eV. Factors like thermal broadening, **k**-point sampling, and finite-size effects discussed in Refs. 35–38 play a role in employing the KGF.

To obtain representative low-energy configurations, atomic structure relaxation of the Cu/G/Cu models was performed. The initial and final Cu–G distances after relaxation are tabulated in the first and second columns of Table I, respectively. It is apparent that the extent of repulsion of Cu atoms away from the graphene is higher for models with short Cu–G distances, indicated by larger shift in Cu–G layers (the third column of Table I). For long Cu–G distances (up to $d_{Cu-G} = 2.61$ Å), most of the Cu–Cu bonds are virtually unaffected, and only few Cu–Cu bonds are formed up to ≈2.52 Å, whereas for short Cu–G distances, the vertical Cu–Cu bonds are also formed at ≈2.49 and ≈2.46 Å.

KGF conductivity for the Cu/G/Cu models in the direction normal to the graphene layer (i.e., along the c-axis in Fig. 1) was computed. Figure 2(a) displays conductivities for the models with different Cu–G distances normalized by the KGF conductivity of the copper crystal computed at 300 K corresponding to $d_{Cu-Cu} = 2.56$ Å. From

TABLE I. Variation in the Cu–G distance for different Cu/G/Cu models after atomic structure relaxation and corresponding transverse component of the stress tensor.

d_{Cu-G}[a] (Å) (Initial)	d_{Cu-G} (Å) (Relaxed)	Shift (Å)	P_z[b] (GPa)
3.22	3.25	0.03	1.7
2.88	2.94	0.06	2.7
2.71	2.78	0.07	3.2
2.54	2.61	0.07	3.1
2.37	2.46	0.09	4.2
2.20	2.37	0.17	6.5
2.02	2.29	0.27	10.3
1.86	2.23	0.37	14.9
1.69	2.19	0.50	20.2

[a]d_{Cu-G} corresponds to the Cu–G distance as shown in Fig. 1(a).
[b]Transverse component of the stress tensor.

Fig. 2(a), we see that the conductivity increases with decreasing Cu–G distance in an almost exponential manner up to $d_{Cu-G} = 2.37$ Å. Beyond 2.37 Å, there is a sharp rise in conductivity followed by a saturation below ≈2.23 Å. The increase in conductivity may be attributed to increased constructive overlapping of copper and graphene orbitals with decreasing Cu–G distance. For the short Cu–G distances with $d_{Cu-G} = 2.23$ Å and beyond, the conductivity is obtained to be ≈10% higher compared to that of copper computed at 300 K. To explore such an increasing trend in the conductivity, we performed Bader charge analysis to compute net charge on the interfacial Cu atoms and the C atoms of graphene and are shown in Fig. 2(b). From Fig. 2(b), we can see that the net charge on C atoms increases, and the net charge on Cu atoms decreases on interfacial Cu atoms with decreasing Cu–G distance. This indicates an increasing charge transfer between interfacial Cu atoms and the graphene with decreasing Cu–G distance. To further understand the electronic structure of these composites with varying Cu–G distance, we computed total EDOS (TDOS) and the projected EDOS (PDOS) on C atoms for selected models and are shown in Fig. 2(c). From Fig. 2(c), we find relatively higher EDOS near the Fermi level with decreasing Cu–G distance. Such an increase in the EDOS is contributed by both copper and carbon atoms of the Cu–G composites, which are more pronounced for short Cu–G distances. The Fermi level also gets shifted toward the conduction band with decreasing Cu–G distance that allows more electronic states to participate for conduction. According to Ref. 39, the DC conductivity, $\sigma_{dc} \propto (N(\varepsilon_f))^2$, where N represents the density of states. So, one expects enhancement of conductivity at short Cu–G distances for these composites as a combined effect of enhanced EDOS near the Fermi level. We note that it was not at all obvious that the graphene would enhance the EDOS at the Fermi level, and we conjecture that this is what underlies experiments showing improved conductivity of the composites.

Further exploration was made by investigating a spatial description of conductivity as a function of the Cu–G distance. We computed the SPC for selected Cu/G/Cu models and are shown in Fig. 3. Figure 3 displays the SPC projected on the 100 plane as a RGB colormap for four such models with different Cu–G distances. The colorbar on the left depicts the magnitude of SPC values, where red color represents low SPC values and blue color represents high SPC values. From Fig. 3, it is apparent that the contribution from both Cu and graphene to the conduction increases with decreasing Cu–G distance and is more significant at short distances. The SPC plots at short Cu–G distances show that the graphene directly participates in conduction and forms a bridge for conduction between Cu atoms on opposite layers.

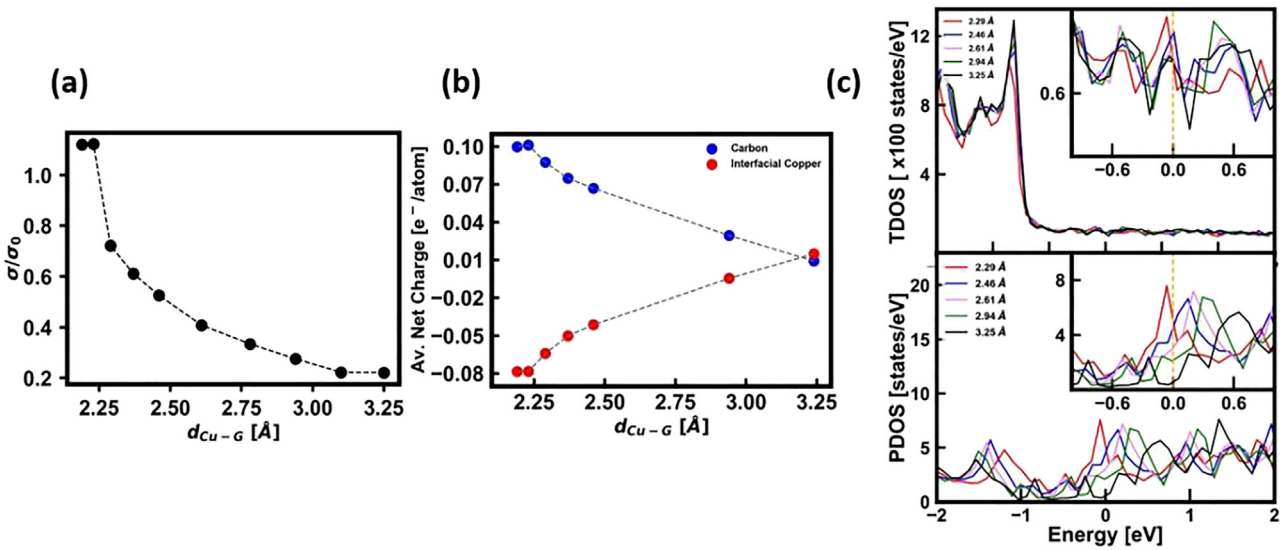

FIG. 2. (a) KGF conductivities for relaxed Cu/G/Cu models with different Cu–G distance normalized by the KGF conductivity (σ_0) of a copper crystal computed at 300 K with $d_{Cu-Cu} = 2.56$ Å. (b) Net charge per atom on interfacial copper atoms (solid red circles) and carbon atoms of graphene (solid blue circles). The dashed lines in subplots (a) and (b) are guide to the eye. (c) Electronic density of states for different Cu/G/Cu models computed at $4 \times 4 \times 2$ **k**-point meshes. The top subplot corresponds to the total EDOS (TDOS), and the bottom subplot corresponds to the projected EDOS (PDOS) onto carbon atoms. The compression of models resulted in an enhanced EDOS near the Fermi level, see the inset for details.

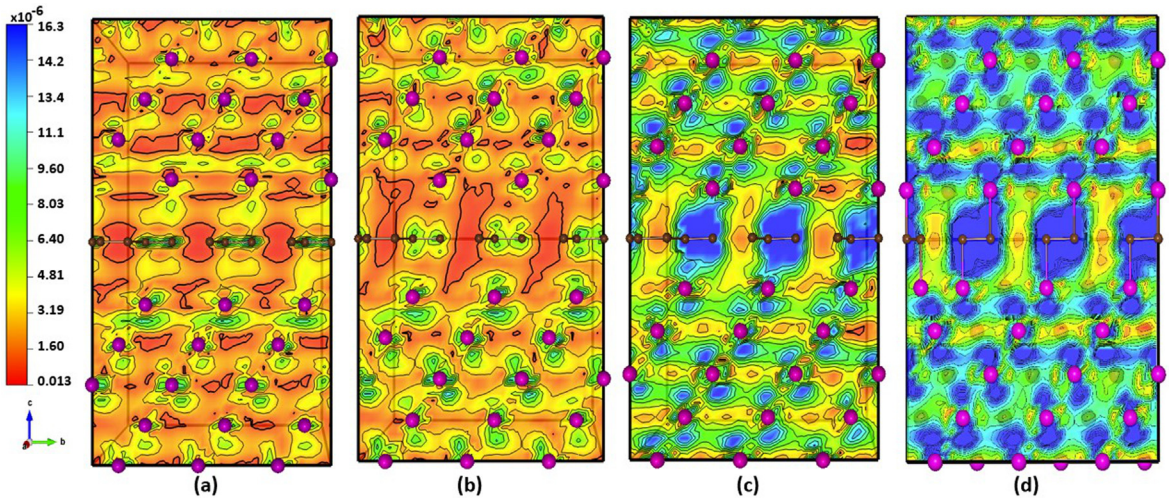

FIG. 3. Space-projected conductivity plotted as a RGB colormap along a plane normal to the graphene for different Cu/G/Cu models corresponding to $d_{Cu-G} = 3.25$, 2.94, 2.29, and 2.23 Å. The colorbar on the left represents the magnitude of SPC values that increases from red toward blue. The SPC values are scaled from the minimum value for $d_{Cu-G} = 3.25$ Å. Cu and C atoms are represented by pink and brown-colored spheres, respectively.

In addition to the graphene, we also see significant contributions from Cu atoms to conduction at short Cu–G distances. This contribution from Cu atoms to the conductivity can be associated with different Cu bonding environments in the Cu–G composites.

KGF conductivity for the orthorhombic Cu model for different vertical Cu–Cu distances ranging from 2.43 to 2.55 Å is calculated and is shown in Fig. 4. From Fig. 4, we can see that the conductivity of Cu increases with reducing Cu–Cu distance from ≈2.55 to ≈2.46 Å after which it drops at ≈2.44 Å. We observed that for short Cu–G distances ($d_{Cu-G} \leq 2.23$ Å), the Cu–Cu bond lengths are also formed at ≈2.49 and ≈2.46 Å. So, the contribution to the conductivity from the Cu atoms with the nearest neighbors close to 2.46 and 2.49 Å is higher compared with Cu atoms at other distances and in agreement with SPC plots in Fig. 3.

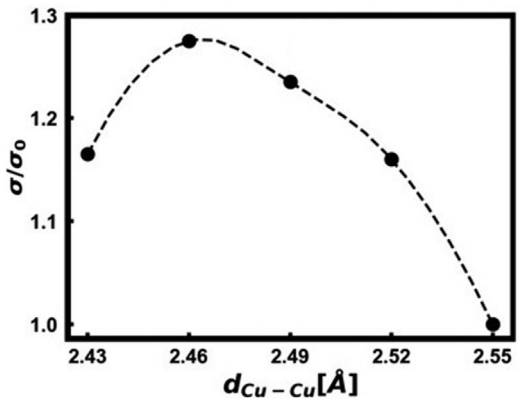

FIG. 4. Relative conductivity (σ/σ_0) of the orthorhombic Cu model computed as a function of the vertical Cu–Cu bond length normalized by the KGF conductivity (σ_0) of a copper crystal computed at 300 K with $d_{Cu-Cu} = 2.56$ Å. The dashed line is a guide to the eye.

Saturation in conductivity of the Cu/G/Cu model for compression below $d_{Cu-G} = 2.23$ Å [refer to Fig. 2(a)] was observed. Such a characteristic is attributed to the contribution of the Cu atoms forming different nearest-neighbor distances. At $d_{Cu-G} = 2.23$ Å, the repulsion of Cu layers on both sides of graphene leads to formation of Cu–Cu bonds at ≈2.49 and ≈2.46 Å. With further reduction in the Cu–G distance, here $d_{Cu-G} = 2.19$ Å, and the Cu–Cu bonds are formed at ≈2.46 Å and also at ≈2.44 Å. So, the additional disorder in Cu leads to slightly less contribution from the Cu atoms to the conduction (refer to Fig. 4) even as the graphene still contributes.

In conclusion, Cu–G composites were modeled by considering the Cu/G/Cu interface model with varying Cu–G distance. We showed that the DC conductivity of the Cu/G/Cu interface models increases with decreasing Cu–G distance, and such an increase is combined contributions from both Cu atoms and the graphene. We attribute this to an enhanced EDOS near the Fermi level. We quantified an increasing charge transfer between interfacial Cu atoms and the graphene with decreasing Cu–G distance. We also provided the spatial view of the electronic conductivity by computing the SPC for varying Cu–G distance. The SPC calculations showed that graphene forms the bridge to electronic conduction between Cu atoms at the interfacial layers. We also showed an interesting characteristic of saturation of the conductivity at a short Cu–G distance (below $d_{Cu-G} = 2.23$ Å), and such a characteristic is mostly attributed to slightly reduced contribution to the conduction from Cu atoms that form Cu–Cu bonds at ≈2.44 Å even when the graphene showing enhanced contribution.

This paper provided one of the first demonstrations of graphene participating in the conduction process along with the Cu atoms in the composite, especially at low Cu–G distances. An implication of this finding is that manufacturing process conditions may influence the electrical performance of metal-graphene composites by engineering the interfaces to encourage graphene's participation in the conduction processes, rather than leaving it as a scattering site. It is important to note that in addition to the interfacial distance, the arrangement of

copper–carbon atoms (geometry) can also influence electrical performance of the composite; however, those effects were not explored in this work. Additional factors of importance, such as the number of graphene layers, their dimensions, and the defect density of the graphene additives, will be explored in the future work. Large scale modeling of the composites can also be benefited from other approaches such as machine learning interatomic potentials trained on short *ab initio* molecular dynamics.[40]

We acknowledge the Extreme Science and Engineering Discovery Environment (XSEDE), supported by NSF via Grant No. ACI-1548562 at the Pittsburgh Supercomputing Center, for providing computational resources under Allocation No. DMR-190008P, the Department of Energy Advanced Manufacturing Office, and the Pacific Northwest National Laboratory operated by the Battelle Memorial Institute for the U.S. Department of Energy under Contract No. DE-AC06-76LO1830.

AUTHOR DECLARATIONS

Conflict of Interest

The authors have no conflicts to disclose.

Author Contributions

Kashi N. Subedi: Formal analysis (equal); Methodology (equal); Writing – original draft (equal); Writing – review & editing (equal). **Kishor Nepal:** Visualization (equal); Writing – review & editing (equal). **Chinonso Ugwumadu:** Writing – review & editing (supporting). **Keerti Kappagantula:** Conceptualization (equal); Supervision (equal); Writing – review & editing (equal). **David A. Drabold:** Conceptualization (equal); Supervision (equal); Writing – review & editing (equal).

DATA AVAILABILITY

The data that support the findings of this study are available from the corresponding author upon reasonable request.

REFERENCES

[1]F. Heringhaus and D. Raabe, "Recent advances in the manufacturing of copper-base composites," J. Mater. Process. Technol. **59**, 367–372 (1996).
[2]O. Bouaziz, H. S. Kim, and Y. Estrin, "Architecturing of metal-based composites with concurrent nanostructuring: A new paradigm of materials design," Adv. Eng. Mater. **15**, 336–340 (2013).
[3]S. Bruschi, J. Cao, M. Merklein, and J. Yanagimoto, "Forming of metal-based composite parts," CIRP Ann. **70**, 567–588 (2021).
[4]M. K. Singh and R. K. Gautam, "Mechanical and tribological properties of plastically deformed copper metal matrix nano composite," Mater. Today: Proc. **5**, 5727–5736 (2018).
[5]L. Weiping, L. Delong, F. Qiang, and P. Chunxu, "Conductive enhancement of copper/graphene composites based on a high-quality graphene," RSC Adv. **5**, 80428–80433 (2015).
[6]H. Rho, Y. S. Jang, S. Kim, S. Bae, T.-W. Kim, D. S. Lee, J.-S. Ha, and S. H. Lee, "Porous copper-graphene heterostructures for cooling electronic devices," Nanoscale **9**(22), 7565–7569 (2017).
[7]Z. An, J. Li, A. Kikuchi, Z. Wang, Y. Jiang, and T. Ono, "Mechanically strengthened graphene-cu composite with reduced thermal expansion towards interconnect applications," Microsystems Nanoeng. **5**, 20 (2019).
[8]J. Yang, Y. He, X. Zhang, W. Yang, Y. Li, X. Li, Q. Chen, X. Chen, K. Du, and Y. Yan, "Improving the electrical conductivity of copper/graphene composites by reducing the interfacial impurities using spark plasma sintering diffusion bonding," J. Mater. Res. Technol. **15**, 3005–3015 (2021).
[9]J. Hwang, T. Yoon, S. H. Jin, J. Lee, T.-S. Kim, S. H. Hong, and S. Jeon, "Enhanced mechanical properties of graphene/copper nanocomposites using a molecular-level mixing process," Adv. Mater. **25**, 6724–6729 (2013).
[10]T. Ellis, I. Anderson, H. Downing, and J. Verhoeven, "Deformation-processed wire prepared from gas-atomized Cu-Nb alloy powders," Metallurgical Trans. A **24**, 21–26 (1993).
[11]D. M. Felicia, R. Rochiem, and S. M. Laia, "The effect of silver (Ag) addition to mechanical and electrical properties of copper alloy (cu) casting product," AIP Conf. Proc. **1945**, 020075 (2018).
[12]D. Kuhlmann-Wilsdorf, "Theory of plastic deformation: Properties of low energy dislocation structures," Mater. Sci. Eng.: A **113**, 1–41 (1989).
[13]K. S. Kappagantula, J. A. Smith, A. K. Nittala, and F. F. Kraft, "Macro copper-graphene composites with enhanced electrical conductivity," J. Alloys Compd. **894**, 162477 (2022).
[14]C. Pan, A. P. S. Gaur, M. Lynn, M. P. Olson, G. Ouyang, and J. Cui, "Enhanced electrical conductivity in graphene-copper multilayer composite," AIP Adv. **12**, 015310 (2022).
[15]L. Zheng, H. Zheng, D. Huo, F. Wu, L. Shao, P. Zheng, Y. Jiang, X. Zheng, X. Qiu, Y. Liu *et al.*, "N-doped graphene-based copper nanocomposite with ultra-low electrical resistivity and high thermal conductivity," Sci. Rep. **8**, 9248 (2018).
[16]C. M. Orofeo, H. Hibino, K. Kawahara, Y. Ogawa, M. Tsuji, K.-I. Ikeda, S. Mizuno, and H. Ago, "Influence of Cu metal on the domain structure and carrier mobility in single-layer graphene," Carbon **50**, 2189–2196 (2012).
[17]L. Banszerus, M. Schmitz, S. Engels, J. Dauber, M. Oellers, F. Haupt, K. Watanabe, T. Taniguchi, B. Beschoten, and C. Stampfer, "Ultrahigh-mobility graphene devices from chemical vapor deposition on reusable copper," Sci. Adv. **1**, e1500222 (2015).
[18]R. Kubo, "Statistical-mechanical theory of irreversible processes. I. General theory and simple applications to magnetic and conduction problems," J. Phys. Soc. Jpn. **12**, 570–586 (1957).
[19]D. A. Greenwood, "The boltzmann equation in the theory of electrical conduction in metals," Proc. Phys. Soc. **71**, 585–596 (1958).
[20]R. M. Martin, *Electronic Structure* (Cambridge University Press, Cambridge, 2008).
[21]P. B. Allen and J. Q. Broughton, J. Phys. Chem. **91**, 4964 (1987).
[22]G. Galli, R. M. Martin, R. Car, and M. Parrinello, Phys. Rev. Lett. **63**, 988 (1989).
[23]G. Henkelman, A. Arnaldsson, and H. Jónsson, "A fast and robust algorithm for bader decomposition of charge density," Comput. Mater. Sci. **36**, 354–360 (2006).
[24]W. Tang, E. Sanville, and G. Henkelman, "A grid-based bader analysis algorithm without lattice bias," J. Phys.: Condens. Matter **21**, 084204 (2009).
[25]K. Prasai, K. N. Subedi, K. Ferris, P. Biswas, and D. A. Drabold, "Spatial projection of electronic conductivity: The example of conducting bridge memory materials," Phys. Status Solidi: Rapid Res. Lett. **12**, 1800238 (2018).
[26]K. N. Subedi, K. Kappagantula, F. Kraft, A. Nittala, and D. A. Drabold, "Electrical conduction processes in aluminum: Defects and phonons," Phys. Rev. B **105**, 104114 (2022).
[27]R. Thapa, C. Ugwumadu, K. Nepal, J. Trembly, and D. A. Drabold, "*Ab initio* simulation of amorphous graphite," Phys. Rev. Lett. **128**, 236402 (2022).
[28]K. N. Subedi, K. Prasai, M. N. Kozicki, and D. A. Drabold, "Structural origins of electronic conduction in amorphous copper-doped alumina," Phys. Rev. Mater. **3**, 065605 (2019).
[29]K. N. Subedi, K. Prasai, and D. A. Drabold, Phys. Status Solidi B **258**, 2000438 (2021).
[30]T. L. Yang, L. Yang, H. Liu, H. Zhou, S. Peng, X. Zhou, F. Gao, and X. T. Zu, "*Ab initio* study of stability and migration of point defects in copper-graphene layered composite," J. Alloys Compd. **692**, 49–58 (2017).
[31]N. A. Lanzillo, J. B. Thomas, B. Watson, M. Washington, and S. K. Nayak, "Pressure-enabled phonon engineering in metals," Proc. Natl. Acad. Sci. U.S.A. **111**, 8712–8716 (2014).
[32]G. Kresse and J. Hafner, "*Ab initio* molecular dynamics for liquid metals," Phys. Rev. B **47**, 558–561 (1993).
[33]P. E. Blöchl, "Projector augmented-wave method," Phys. Rev. B **50**, 17953–17979 (1994).

[34]J. P. Perdew, K. Burke, and M. Ernzerhof, "Generalized gradient approximation made simple [Phys. Rev. Lett. 77, 3865 (1996)]," Phys. Rev. Lett. **78**, 1396–1396 (1997).
[35]A. Belmonte *et al.*, "Operating-current dependence of the Cu-mobility requirements in oxide-based conductive-bridge RAM," IEEE Elec. Devices Lett. **36**(8), 775–777 (2015).
[36]D. Knyazev and P. levashov, Comput. Mater. Sci. **79**, 817 (2013).
[37]L. Calder'm, V. Karaseiv, and S. Trickey, Comput. Phys. Commun. **221**, 118 (2017).
[38]P. Bulanchuk, "On the delta function broadening in the Kubo-Greenwood equation," Comput. Phys. Commun. **261**, 107714 (2021).
[39]N. Mott and E. Davis, *Electronic Processes in Non-Crystalline Materials*, 2nd ed. (Clarendon Press, Oxford, 1979).
[40]B. Mortazavi, E. V. Podryabinkin, S. Roche, T. Rabczuk, X. Zhuang, and A. V. Shapeev, "Machine-learning interatomic potentials enable first-principles multiscale modeling of lattice thermal conductivity in graphene/borophene heterostructures," Mater. Horiz. **7**, 2359–2367 (2020).